An experimental set up to study the micro-mechanisms of stress corrosion cracking

L. Stermann[a], G. Simon, R. Fulcrand, L. Vanel and D. Tanguy[b]

Institut Lumière Matière (ILM) - CNRS : UMR5306, Université de Lyon - UCBL 1 - France
a. leonel.stermann@univ-lyon1.fr
b. dome.tanguy@univ-lyon1.fr

Résumé :

Un montage expérimental est présenté. Il est conçu pour l'étude de la fissuration par corrosion sous contrainte, à petite échelle, à partir de micro entailles. Les échantillons ont une taille intermédiaire entre les éprouvettes polycristallines classiques (quelques mm) et les micro-poutres (10 μm). La technique de "corrélation d'images numériques" (CIN) est utilisée pour quantifier la déformation plastique induite par le chargement mécanique nécessaire à l'amorçage de la fissuration depuis le fond d'entaille. Les champs de déplacement élastiques sont aussi mesurés et calculés par "éléments finis" pour obtenir le facteur d'intensité des contraintes (K). La plasticité introduite par le chargement mécanique initial est faible: moins de 0.5% à la pointe de l'entaille, et moins de 0.2% dans le reste de l'échantillon. Les premiers essais de fissuration donnent des valeurs de K entre 4 et 6 MPa$\sqrt{m}$, en accord avec la littérature. La nature intergranulaire de la fissuration est confirmée par des observations en microscopie à balayage de faciès de rupture.)

Abstract :

An experimental set-up is presented. It aims at studying stress corrosion cracking in a U-notch aluminum alloy sample at a small scale, intermediate between the polycrystal (1mm) and the micro beam (10μm). Digital Image Correlation (DIC) is used to determine the amount of plasticity introduced before crack initiation from the notch tip. The elastic displacement field is also measured by DIC, and numerically calculated, in order to obtain the Stress Intensity Factor (SIF) during crack propagation. The plasticity introduced, at the load level necessary for obtaining initiation, is negligible. It is less than 0.5% at the tip of the notch and less than 0.2% for the rest of the sample. First stress corrosion cracking results show that the SIF values during crack propagation are in between 4 and 6 MPa$\sqrt{m}$, being consistent with a SCC intergranular brittle fracture according to the literature. The intergranular nature of the crack is confirmed by a SEM observation of the final fracture surface.

Key words : Stress Corrosion Cracking, Aluminum Alloys, Intergranular Fracture, Micromechanics

1 Introduction

Stress Corrosion Cracking (SCC) has an important impact on economy because it causes safety issues which impose frequent inspections and repair of structures. Despite many efforts, a consensus on the essential mechanisms have not been achieved yet. The existing models have limited predictive capabilities and rely on the phenomenology specific of the system under consideration. Understanding the physics of the processes involved is necessary but the progress in this direction have not reached the extent where a new generation of models can be developed. One reason is the variety and complexity of the phenomena involved. For example, in aqueous SCC, the predominant role played by hydrogen has been demonstrated but many essential questions remain. Indeed, Hydrogen is produced by electrochemical reactions at the surface, penetrates in the material and interacts with the microstructure. But there are still debates on how H causes decohesion and what is its interplay with the plastic deformation, which process results in crack nucleation and propagation. Different strategies exist to tackle these issues. One consists in observing crack propagation, at the grain scale, on real industrial materials and environments, and modeling it using continuum simulations such as polycristalline agregates with crystalline plasticity [1, 2, 3] and phenomenological rules. Others consist in reducing the size of the system by using micromechanical devices [4], such as flexion microbeam [5] and nanoindenters, or FIB scliced samples on pre-exposed materials[6]. Then fracture is characterized at a fine scale with high resolution SEM, post mortem TEM or APT. Our goal is to develop an exprimental set-up to study crack propagation at a small scale, intermediate between the polycristal (1mm) and the micro beam (10μm). Such a scale should be appropriate for using the sample itself as a hydrogen reservoir for the duration of the fracture test, in an environment where a corrosive cell cannot be used, the vacuum of scanning electron microscope for example. At the same time, it should be small enough to have a reduced number of grains along the crack front, such that the analysis of the impact of the crystallography on the fracture processes be simplified with respect the polycristalline approach. The objective is to follow the crack with an in-situ measure of crack tip plasticity and a sub-grain size scale.

The paper is organized as follows. A first part gives an overview of the set up, then a second part reports the tests that where done to quantify the mechanical load which is applied to the sample and to measure which accuracy can be reached for the measurement of the plastic field. Finally, an example of a stress corrosion test, followed in situ under an optical microscope is given.

2 Experimental set up

A material and a sample design were chosen to favor fast single intergranular cracking. The material is a rolled plate of aluminum alloy AA7108 (AlZnMg with low Cu content, sensitive to SCC) for which the grains exhibit a strong morphological texture with the grains elongated in the rolling direction. The samples are heat treated 1 hour at 400 C and water quenched (T4 state) because it was shown that they were sensitive in this metallurgical state [9] with a microstructure which consists in small clusters of Zn and Mg (precursors of the $MgZn_2$ hardening phase). No intergranular $MgZn_2$ precipitates are present [8]. The micro traction samples are oriented in the short transverse direction to take advantage of this texture. It has an overall length of 8 mm (plate thickness) and a gage length of 4 mm. The width and thickness are 1 mm. The gripping device is an in-house made aluminum frame shown in Figure 1 (a). A single edge U-notch is machined at the length center with a high cutting speed. It has 60 micron radius and 300 micron length. Its role is to favor single cracking by concentrating the stress and localizing the plastic deformation, in the initiation stage of cracking. The sample is polished to a mirror state in order

to be observed under a microscope.

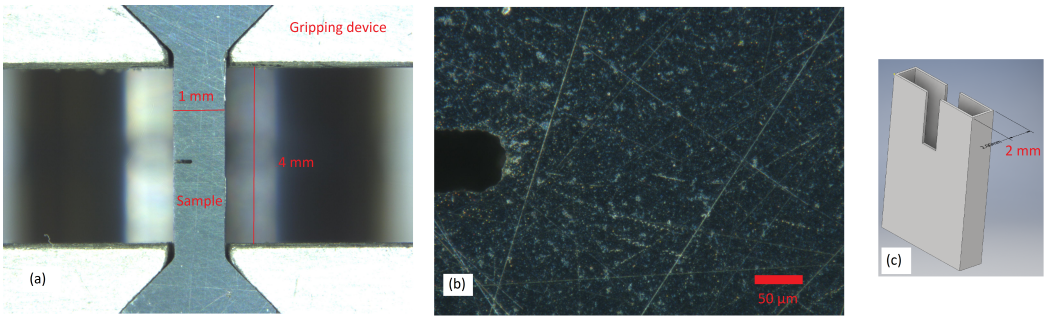

Figure 1: (a) The tensile sample are oriented along the short transverse direction of the rolled plate they were extracted from. Their length is the thickness of the plate. The figure shows also the grips used.(b) Sample surface and notch tip at maximum magnification (x112).(c) Saline water container.

A DEBEN micro-traction stage with a force cell of maximum capacity 660 N is used. As a first approach, the micro traction machine is fixed to the base of a Stereo Microscope Zeiss that allows magnifications between 7x and 112x with an IDS camera (2560 x 1920 pixels). It uses a ring illuminator that brings homogeneous illuminations for large object fields. It also has a large working distance that allows to traction the sample without risking the optical system. In addition, the displacement field on the side surface can be measured by Digital Image Correlation (DIC), giving the possibility to measure precisely the elastic field, and therefore the stress intensity factor, and also the extent of the plastic zone[7]. The necessary pattern for DIC comes from surface heterogeneities, revealed by the polishing and the contrast created by the reflection angle of incident ring light. Figure 1 (b) shows a sample surface at x112 (maximum magnification).

As a first step, the embrittlement is obtained by immersing the notch in a saline solution (NaCl 30g/l). The sample itself is not fully immersed. The top surface is only exposed to air and is used, in the absence of corrosive attack, to generate the pictures used in DIC. For this, a millimeter size container, built from a 3D printer (Figure 1 (c)), is mounted on the sample. It brings saline water in contact with the notch, which is left at free electrochemical potential during the constant load test.

Finally, it is planned to characterize the crystalline orientation of the grains on the surface by EBSD before testing. It should reveal the intergranular path, on the surface of the sample, give the orientation of the grains with respect to the traction axis from which the active slip planes should be identified. The morphological texture, if the grains do not recrystallize during the preparation of the sample (Figure 3 (b)), should favor planar crack through the grain boundaries which are perpendicular to the traction axis. Therefore, the knowledge of the orientation of grains from EBSD and the known orientation of the GB plane are enough information to characterize the crystallographic nature of the interfaces (except from a relative rigid body translation of the grains).

2.1 Digital Image Correlation

Digital image correlation analysis is carried out using a free suite of python tools called Pydic [13], based on the library OpenCV. Pydic is implemented to measure the displacement field on the sample surface from two pictures, and from this data calculate the strain tensor. Pydic creates a correlation grid in order to find the displacement of each grid point. The spatial resolution can not be better than the grid size, 10x10 pixels in our case. The "Lucas Kanade feature tracker" from Bouguet [15] as

implemented in OpenCV, was used. Rigid body translation is eliminated. The strain calculation involves, a B-spline interpolation method for the displacement field and a numerical differentiation, obtaining all the components of the strain tensor.

In order to observe the whole gage length in a single picture, it is necessary to use a low magnification x13 (1.7 μm/pixel). This low magnification limits the spatial resolution, to approximately 17 μm due to grid size (10x10 pixels). Furthermore, in order to follow the crack during propagation, the maximum magnification x112 (0.18 μm/pixel) is used. Then, the best spatial resolution is 1.8 μm, which is close to the order of magnitude of the length scale of the pattern (Figure 3 (a)).

2.2 Displacement and Strain Fields

Initiating a SCC crack from a U-notch requires mechanical overloading. Our preliminary tests show that the force range for crack initiation is in between 70N and 100N. It is important to quantify the amount of plasticity introduced by this overloading in the bulk of the sample as well as at the notch tip. Indeed, it is well know that plastic deformation is essential to trigger electrochemical reactions at the notch tip that would induce crack nucleation. On the other hand, the goal is to characterize the amount of plasticity accompanying SCC propagation. It is necessary that the initial overloading does not create a large plastic deformation in the whole sample. In the following, the procedure to measure the plastic and elastic components of the displacement field is detailed together with results concerning the evaluation of K_I

There are three different types of displacement fields. The total displacement field is the sum of the elastic displacement and the plastic displacement. The elastic displacement is reversible after the stress is removed; on the contrary; plastic displacement is permanent. To measure these fields, sample images are correlated at specific stages during the tensile test. Furthermore, the previous statement also is true for strain fields. In addition, a notch is a stress raiser and also inducing bending in the sample [11]. Another bending cause is a misalignment in the gripping device used to transmit the force [10]. Because of these reasons, strain is not uniform in the sample and the displacement fields are complex.

Measurements of the displacement fields are illustrated with an example: the deformation caused by an increment of the force from 0N to 85N. First, the total deformation is measured using the correlation between image A obtained from a force free sample and image B where the sample is submitted to a force of 85N. Second, the elastic displacement is measured due to the elastic recovery, as the correlation between the sample image B and the subsequent complete removal of the force, coming back to 0N (image C). Finally, the plastic displacement is obtain as a direct correlation between images C and A.

In the 85N force example, plastic strain in the tensile direction is very low in the sample. It is only higher than 0.05% in a small area in the central zone of the sample, near to the notch, achieving a maximum of 0.1% at the notch tip. Moreover, in the case of the highest force in the study range (100N), the plastic strain is not even 0.5% at notch tip, while being below 0.2% in the rest of the sample. With these low levels of plasticity we can consider a macroscopic elastic behaviour. The associated plastic displacement field mainly presents bending deflection and notch opening. It is important to know the magnitude of the local plastic strain increment corresponding to a force increment. We measured the plastic displacement field increment corresponding to a force increase from 85N to 100N. The requisite is to pre-strength the sample up to 85N and then return to a zero force state before starting the DIC test, in order to avoid any remainder of elastic field. Figure 2 (b) illustrates with arrows the measured plastic field (magnified by a factor 40). Two main features can be seen: the notch opening and the bending deflection. Because

of notch opening, the arrows at the middle of the figure (notch plane) points in the notch direction (the notch is on the right side) with a low vertical component. Then, the vertical component increases rapidly near notch tip.From the presented plastic displacement field (Figure 2 (b)), the strain field is calculated and mapped on the sample surface in Figure 2 (a). Compression and elongation zones can be clearly identified. The zones in small compression might be due to bending. The hottest spot (maximum strain) is located at the notch tip, revealing opening and 0.3% of plastic strain. The notch is surrounded by concentric semi circles of lower strain values (stress raiser effect), creating a plastic gradient which extends over 100 μm ahead of the notch.

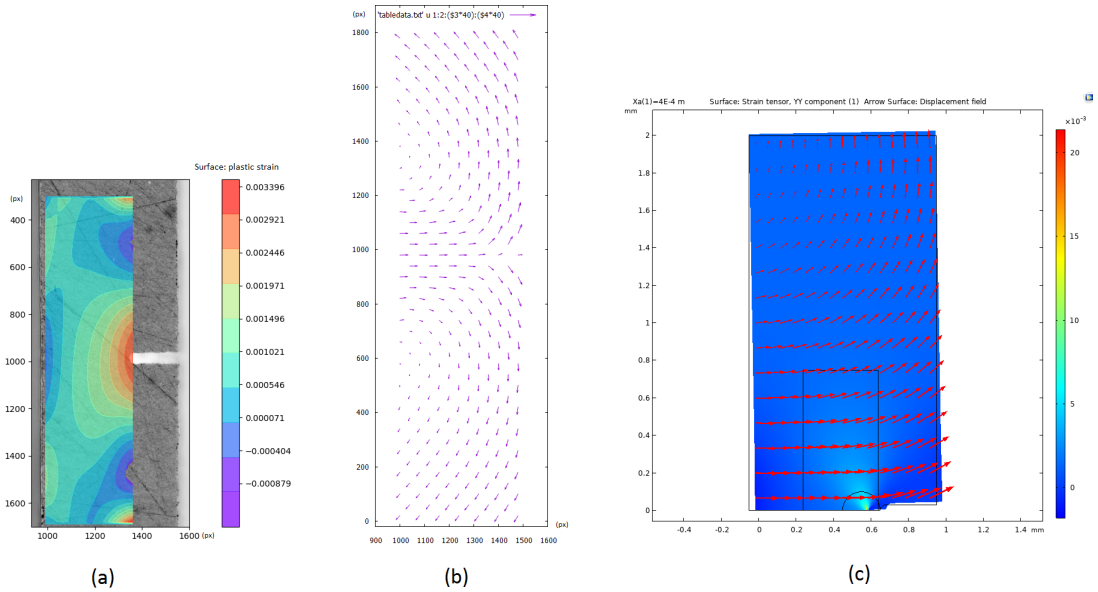

Figure 2: (a) Plastic strain ε_{yy} map from(b) plastic displacement field by DIC from 85 to 100N increment force.(c) FEA-COMSOL elastic calculation used for the J integral, the energy release rate and the stress intensity factor, at 100N applied force. The deformed body, the elastic displacement field with red arrows and a ε_{yy} color-map are illustrated.

The elastic displacement field is important to determine the stress intensity factor. It is also possible to compare the experimental elastic fields with the calculated ones by FEA using the elastic linear theory. Because the displacement fields are complex, it is convenient to introduce the overall strain $\hat{\varepsilon}$ in a sample. The overall strain $\hat{\varepsilon}$ is the difference of the average displacement(in the traction direction) at the top side and at the bottom side, divided by the gage length. It is analogous to the engineering strain for a tensile test.

The elastic displacement is measured by unloading the sample, correlating image B with image C. The strain distribution is not homogeneous due the presence of the notch. The overall strain $\hat{\varepsilon}$ is 0.15% for a 100N applied force. In addition, FEA-COMSOL calculation were made (Figure 2 (c)) and the value of overall strain $\hat{\varepsilon}$ is 0.15%, in agreement with the DIC measure. Moreover, both displacement fields (numerical and experimental) show bending deflection and notch opening. .(Figure 2 (c)) shows with red arrows the elastic displacement field and the deformed shape of the sample. The stress intensity factor is also calculated in this COMSOL simulation using two different methods, described below.

The J integral is computed with three 2D integration paths. In addition, the energy release rate G is also calculated by computing the potential energy difference for two slightly different crack lengths, during a virtual crack propagation. The two methods are in excellent agreement. Linear fracture mechanics

gives $K_I^2/E = J = G\,K_I$ is 5.5 MPa $\sqrt{m}$ for an applied force of 100N when a 30 μm crack emerging from the notch tip is considered.

Finally, a last experience related to the elastic field is presented in this section. The elastic component of the displacement field is measured during the crack propagation in a SCC test, using the maximum magnification (x112). One picture is taken when the force is still applied, and the second one after the complete removal of the applied force (Stage B vs Stage C). The experimental elastic displacement field by DIC was compared to a theoretical elastic displacement field created by a classical Griffith-Inglis crack (finite crack in an infinite body) in Mode I. Using least squares fitting method, an approximate value of 4 MPa $\sqrt{m}$ is obtained [12] with no detection of mode II. Even if the sample bends, no mode II is found, as in the case of three-point bending. [7][14]

3 Stress Corrosion Cracking Test

During the SCC test, the sample is under a constant tension value, and the saline solution is in an intimate contact with the notch tip. The typical initiation time to obtain a visible crack is about 4 hours, setting a 100N constant force. The crack propagation is followed with the stereoscopic microscope, as can be seen in Figure 3 (a) where a single crack initiates from the notch tip (saline water is seen inside the notch). It propagates in the direction perpendicular to the applied force. Due to plastic deformation or water invading the sample surface, a bright contrast is created during the crack. Its interpretation is not clear. This issue might be might solved by depositing a transparent hydrophobic layer.

In order to arrest completely the crack during crack propagation, the applied force must drop to a value below 40N (approx 3 MPa $\sqrt{m}$). If the crack is not arrested by reducing the force, the total crack propagation time is less than two hours for a complete sample failure. Figure 3 (b) is a SEM image, the left side is the notch and the right side is the fracture surface that confirms a brittle intergranular crack.

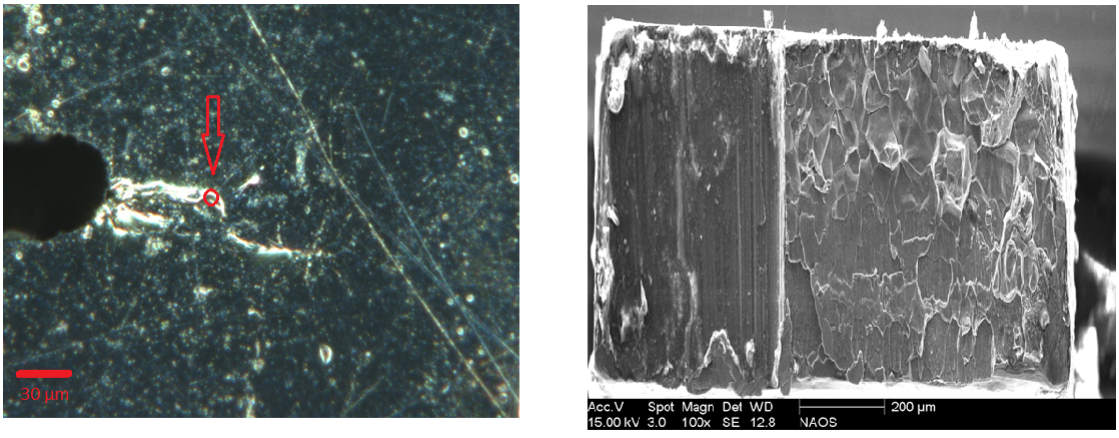

(a) (b)

Figure 3: (a) Stereo microscope image of SCC crack propagation from the tip of the notch on the sample surface, the crack tip is highlighted in red (b) SEM image of the final fracture surface

4 Conclusion

Plastic and elastic displacement have been measured by DIC in the force range where crack initiation takes place for SCC test. Strain fields are calculated using interpolation methods from the displacement

fields. Opening Mode I and bending deflection is present. The plastic strain is very low for crack initiation, even at the maximum force in the range, being negligible all over the sample (less than 0.2%), and less than 0.5% at the notch tip for 100N. Measured elastic displacement fields during crack propagation have been used to compute the stress intensity factor, a low value of K_I is consistent with a SCC brittle fracture.

Perspectives: Plastic strain will be measure by DIC during crack propagation, using a higher magnification in an optical microscope. A hydrophobic transparent layer will be deposited, improving the stability in time of the surface state. Consequently, crack tip location will be more precise, improving crack velocity measurement. In the future, the measured displacement will be used as boundaries conditions during finite elements analysis, to improve accuracy.

References

[1] E. Pouillier, A.-F. Gourgues, D. Tanguy, E.P. Busso,, A study of intergranular fracture in an aluminium alloy due to hydrogen embrittlement, Int J. of Plasticity 34, 139-153, 2012.

[2] E. Durif, M. Fregonese et al. Methodology for a mechano-electrochemical evaluation of the coupling at the crack tip. Application of halide-induced Stress Corrosion Cracking of Zircaloy-4, Corrosion Science 93, 39-47, 2015.

[3] I. Aubert and N. Saintier and J.-M. Olive and F. Plessier, A methodology to obtain data at the slip-band scale from atomic force microscopy observations and crystal plasticity simulations. Application to hydrogen-induced slip localization on AISI 316L stainless steel, acta mater. 104, 9-17, 2016.

[4] S. Jaddi and M. Coulombier and J.-P. Raskin and T. Pardoen, Crack on a chip test method for thin freestanding films, Journal of the Mechanics and Physics of Solids 123, 267-291, 2018

[5] Yun Deng and Afrooz Barnoush, Hydrogen embrittlement revealed via novel in situ fracture experiments using notched micro-cantilever specimens, acta mater. 142, 236-247, 2018

[6] H. Dugdale and D. E. J. Armstrong and E. Tarleton and S. G. Roberts and S. Lozano-Perez, How oxidized grain boundaries fail, acta mater. 61, 4707-4713, 2013

[7] S. Roux and F. Hild, Stress intensity factor measurements from digital image correlation: postprocessing and integrated approaches, Int J. Fracture 140, 151, 2006.

[8] Neji Ben Ali. Caractérisation et modélisation micromécanique de la propagation de fissures fragiles par effet de l'hydrogène dans les alliages AA 7xxx. Ecole Nationale Supérieure des Mines de Saint-Etienne, 2011.

[9] N. Ben Ali, D. Tanguy and R. Estevez Effects of microstructure on hydrogen-induced cracking in aluminum alloys Scripta Materialia 65 (2011) 210–213

[10] ASTM International, 8/E8M – 09 Standard Test Methods for Tension Testing of Metallic Materials, 2009, United States

[11] W. D. Pilkey, Formulas for Stress, Strain, and Structural Matrices, Second Edition. John Wiley and Sons, 2005, Chapter 6

[12] J.Weertman, Dislocation based fracture mechanics, World Scientific Publishing, 1996, pp. 17–18.

[13] D. André, Pydic, www.unilim.fr/pages_perso/damien.andre/index.html, Universite de Limoges, (04/02/2019)

[14] ASTM International, E1820 – 13 Standard Test Method for Measurement of Fracture Toughness, 2014, United States

[15] J.-Y. Bouguet, Pyramidal Implementation of the Lucas Kanade Feature Tracker Description of the algorithm, Intel Corporation